

# MECHANO-CHEMICAL SYNTHESIS OF NANOSTRUCTURED HYDRIDE COMPOSITES BASED ON Li-Al-N-Mg FOR SOLID STATE HYDROGEN STORAGE

Robert A. VARIN – Leszek ZBRONIEC – Minchul JANG

**Abstract:** It is observed that large quantities of hydrogen ( $H_2$ ) are released at ambient temperatures during the mechano-chemical synthesis of the Li-Al-N-Mg-based hydride composites using an energetic ball milling in a unique magneto-mill. For the ( $nLiAlH_4+LiNH_2$ ;  $n=1, 3, 11.5, 30$ ) composite, at the molar ratio  $n=1$ , the  $LiNH_2$  constituent destabilizes  $LiAlH_4$  and enhances its decomposition to  $Li_3AlH_6$ , Al and  $H_2$ , and subsequently  $Li_3AlH_6$  to LiH, Al and  $H_2$ .  $LiNH_2$  ceases to destabilize  $LiAlH_4$  in the composites with increasing molar content of  $LiAlH_4$  ( $n \geq 3$ ). For the ( $nLiAlH_4+MnCl_2$ ;  $n=1, 3, 8, 13, 30, 63$ ) composite, XRD phase analysis shows that chemical reaction occurs during ball milling between the hydride and chloride constituent forming either an inverse cubic spinel  $Li_2MnCl_4$  for  $n=1$  or lithium salt (LiCl) for  $n > 1$ . Both reactions release hydrogen. For the ( $LiNH_2+nMgH_2$ ;  $n=1, 1.5$ ) composite the pathway of hydride reactions depends on the milling energy and milling time. Under low milling energy up to 25h there is either no reaction (1h) or the reaction products are amorphous  $Mg(NH_2)_2$  (magnesium amide) and nanocrystalline LiH (lithium hydride) without any release of hydrogen. Under high milling energy a new hydride  $MgNH$  (magnesium imide) is formed due to reaction between  $Mg(NH_2)_2$  and  $MgH_2$  which is always associated with the release of  $H_2$ .

**Keywords:** – hydrogen energy  
– solid state hydrogen storage  
– ball milling  
– hydrogen discharge

## 1. INTRODUCTION

The apparent solution to the looming problem of energy shortage in the 21<sup>st</sup> century is a dramatic cut off in the consumption of fossil fuels in general and crude oil in particular. This could also help in cutting global fossil carbon emissions. The most ideal energy carrier for the future hydrogen economy which can be produced cleanly, cost-effectively and easily converted to electrical energy in fuel cells is hydrogen. In contrast to any other sustainable or renewable energy carrier or source, hydrogen is the most universal one, because it can power automobiles, airplanes, off-road vehicles (e.g. fork lifts), portable electronic devices and stationary back up power systems that are powered by fuel cells. However, a widespread hydrogen use, particularly for transportation or automotive applications, is hindered by three major obstacles: (1) improvement of fuel cells which produce electrical current and water vapor when fuelled by

hydrogen, (2) inexpensive hydrogen production from ideally renewable sources and (3) hydrogen storage. The latter obstacle is most likely the most important one, particularly, for automotive applications. Gaseous and liquid hydrogen storage techniques have a number of serious drawbacks although high pressure (70 MPa) gaseous storage will be the most likely short-term solution (next 10 years or so) for the transportation sector. However, for stationary, portable and off-road mobile as well as for long-term automotive applications, a general consensus emerged that a better option is solid state hydrogen storage in hydrides and their composites. Proton Exchange Membrane (PEM) fuel cell stacks, which are the most suitable for automotive and a number of other applications, generate the amount of waste heat corresponding roughly to 60-100°C temperature range [1]. Therefore, the operating temperature range of a potential hydride-based storage system should exhibit the dehydrogenation temperature compatible with waste heat of a PEM

fuel cell stack. Obviously, the highest possible H<sub>2</sub> capacity of the solid hydride storage system is another important consideration and for 2015, H<sub>2</sub> capacity of 5.5 wt. % for the entire storage system, which includes storage material, tank and some auxiliary devices [2] is required by the recently revised US Department of Energy (DOE) targets. In turn, approximately 10 wt. % H<sub>2</sub> capacity for the solid hydride-based storage material is required. Such large material capacities can only be provided by complex light metal/nonmetal hydrides and most likely by their composites [1].

It is well known that energetic ball milling of hydrides substantially refines their particle size and forms nanometric grains within the particles [1]. In this paper the mechano-chemical synthesis using an energetic ball milling in a unique magneto-mill will be discussed for three selected Li-based composite complex hydride systems: (1) lithium alanate (LiAlH<sub>4</sub>) and lithium amide (LiNH<sub>2</sub>); (2) lithium alanate and manganese chloride (MnCl<sub>2</sub>) and (3) lithium amide and magnesium hydride (MgH<sub>2</sub>). Under the action of mechanical energy, the observed release of hydrogen in these systems is analyzed in terms of mechano-chemical reactions and nanostructure development during ball milling.

## 2. EXPERIMENTAL

Hydride powders such as LiAlH<sub>4</sub> (97% purity), LiNH<sub>2</sub> (purity 95%), MgH<sub>2</sub> (purity 98%) and MnCl<sub>2</sub> (purity 99.99%) were mixed into the following hydride molar ratios: (1) nLiAlH<sub>4</sub>+LiNH<sub>2</sub> (n=1, 3, 11.5 and 30), (2) nLiAlH<sub>4</sub>+MnCl<sub>2</sub> (n=1, 3, 8, 13, 30 and 63), (3) LiNH<sub>2</sub>+nMgH<sub>2</sub> (n=1 and 1.5). The mixtures with various ball-to-powder weight ratios (R) were subsequently composited by controlled ball milling for pre-determined time durations in the magneto-mill Uni-Ball-Mill 5 under high and low milling energy modes. IMP67&68 modes are high impact energy modes with two very strong Nd-Fe-B magnets at 6/8 and 6/7 o'clock positions, respectively, and 4 steel balls in the milling vial. LES6 is a low energy shearing mode with one magnet at 6 o'clock and 2, 3 and 4 steel balls (2, 3 and 4B) (details can be found in [1, 3-7]). The pressure of high purity hydrogen (purity 99.99%: O<sub>2</sub>< 2 ppm; H<sub>2</sub>O< 3 ppm; CO<sub>2</sub>< 1 ppm; N<sub>2</sub>< 6 ppm; CO< 1 ppm; THC< 1 ppm) in the vial was kept constant at ~ 600 kPa during the entire milling process. Ball milling was carried out under continuous cooling of the milling vial by an air fan.

The release of hydrogen during ball milling was estimated from the pressure increase in the milling vial measured by a pressure gage using an ideal gas law [1] and expressed in wt. % with respect to the total weight of powder sample. The powder samples were handled in a glove box always containing a moisture removing Drierite granulated compound. Before handling, the glove box was purged a few times and then filled with high purity argon gas (99.999% purity) in order to minimize any possible contamination by moisture or oxygen from air.

X-ray powder diffraction (XRD) analysis was performed on a Bruker D8 diffractometer using a monochromated CuKα<sub>1</sub> radiation (λ=0.15406 nm) produced at an accelerating voltage of 40 kV and a current of 30 mA. The scan range was from 2θ=10° to 90° and the rate was 1.2° min<sup>-1</sup> with a step size of 0.02°. Powder was loaded in a glove box filled with Ar into a home-made environmental brass holder with a Cu/glass plate for powder support. Upper and lower part of the environmental holder is sealed through a soft-rubber O-ring and tightened using threaded steel bolts with nuts. The upper part of the holder contains a Kapton polymeric tape window transmittable to X-rays.

Ball milling resulted in a substantial refinement of powder particle size and formation of nanometric grains within the particles. The latter can be estimated from the Bragg diffraction peak breadth using X-ray diffraction (XRD) [1, 3-7]. XRD was also used for the phase identification before and after ball milling. The Specific Surface Area (SSA) of the powders in the (LiNH<sub>2</sub>+1.0MgH<sub>2</sub>) system before and after ball milling was measured by the BET (Brunauer, Emmett and Teller) method in the CanmetENERGY, Natural Resources Canada, Ottawa.

## 3. RESULTS

### 3.1. Composite (nLiAlH<sub>4</sub>+LiNH<sub>2</sub>)

Figure 1a shows the quantity of H<sub>2</sub> desorbed during ball milling, plotted as a function of the molar ratio n in the (nLiAlH<sub>4</sub>+LiNH<sub>2</sub>) composite. It is observed that during ball milling up to 30 min the composites with molar ratio n=1 and 3 gradually decompose releasing H<sub>2</sub>. In particular, Figure 1b shows that for n=1 further ball milling up to 3h (180 min) releases about 5 wt.% H<sub>2</sub>. In order to make sure that the results were reproducible the milling tests were repeated twice as shown in Figure 1b (1st and 2nd

run). It is clearly seen that for the composite with  $n=1$ , the quantity of desorbed  $H_2$  is exactly the same for the 1st and 2nd run, which means that the hydrogen quantities desorbed during ball milling are perfectly reproducible. The composites with  $n=11.5$  and greater do not release hydrogen during milling up to 30 min (Figure 1a).

The phase changes occurring during ball milling as a function of milling time and molar ratio were investigated by X-ray diffraction (XRD) of the samples taken after pre-determined milling durations. The XRD patterns are shown in Figure 2. The XRD pattern for the  $n=1$  composite (Figure 2a) shows that after 2 min of milling the diffraction peaks of both constituents  $LiAlH_4$  and  $LiNH_2$  are still clearly observed. There is also a peak of Al,

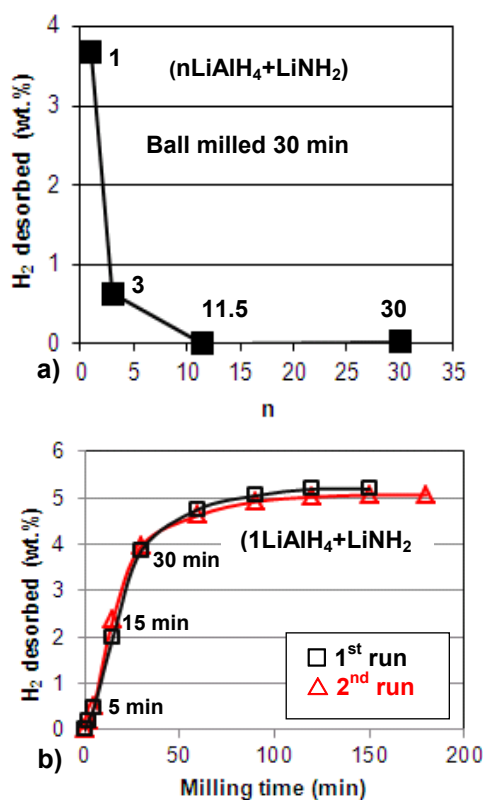


Figure 1. The quantity of  $H_2$  desorbed during ball milling of  $(nLiAlH_4 + LiNH_2)$  as a function of (a) the molar ratio  $n$  (the numbers show the corresponding values of  $n$ ) and (b) milling time for the composite with  $n=1$

which is an impurity in as received  $LiAlH_4$  [8-10]. After 15 min of ball milling the principal peaks of  $Li_3AlH_6$  become much stronger. It must be pointed out that the strong diffraction peaks of  $LiNH_2$  are

still observed which indicates that no chemical reaction between  $LiAlH_4$  and  $LiNH_2$  occurred during ball milling.

As can be seen in Figure 2b, for the  $n=1$  composite with increasing ball milling time to 30 min, 1h and 3h, the peaks become broadened and more diffuse as well as the uprising in the baselines and the formation of a broad “hump” in the range of  $2\theta=30-40^\circ$  are observed which can be attributed to heavy nanostructuring or even the existence of increasing quantities of amorphous structure(s) [11, 12]. The 100% intensity peaks of  $LiAlH_4$ ,  $LiNH_2$  and  $Li_3AlH_6$  are still visible after 30 min and even after 1h of milling although they are much weakened (Figure 2b). There are also clear peaks which we assign to Al. It is interesting that Xiong et al. [11], in their first paper on the ball milling of  $(1LiAlH_4 + LiNH_2)$  (molar ratio  $n=1$ ) reported that the peaks of Al were clearly observed in the XRD patterns of the ball milled samples although they were gradually weakened with milling time. However, in their second paper [12] on the ball milling of  $(0.5LiAlH_4 + LiNH_2)$  (molar ratio  $n=0.5$ ), they reported that no Al peaks were detected during the milling process. In contrast, Dolotko et al. [13] reported that no Al was detected in the  $(1LiAlH_4 + LiNH_2)$  composite during ball milling but instead they concluded that mostly the amorphous AlN compound was formed during ball milling. On that basis, they proposed that a solid state reaction between  $LiAlH_4$  and  $LiNH_2$  occurred during ball milling which resulted in the formation of AlN,  $2LiH$  and  $2H_2$ . The quantity of  $H_2$  released in this transformation is 6.6 wt. % which they claimed to observe as being released after 30 min of ball milling.

However, we believe that the peaks assigned to Al in Figure 2a, b for the milling duration from 2 min to 1h of milling, indeed correspond to Al and not AlN.

The problem here is that the Fm3m space group of Al (JCPDS 85-1327) is identical to AlN (JCPDS 46-1200) which means that practically their XRD diffraction patterns superimpose. However, the intensities of the principal peaks of Al and AlN are opposite. For Al the (111) peak at  $2\theta=38.5^\circ$  and (200) peak at  $2\theta=44.74^\circ$  has 100% and 50% intensity, respectively. For AlN the peak intensity of the (111), (200) and (220) ( $2\theta=65.17^\circ$ ) peak is 30, 100 and 55%, respectively.

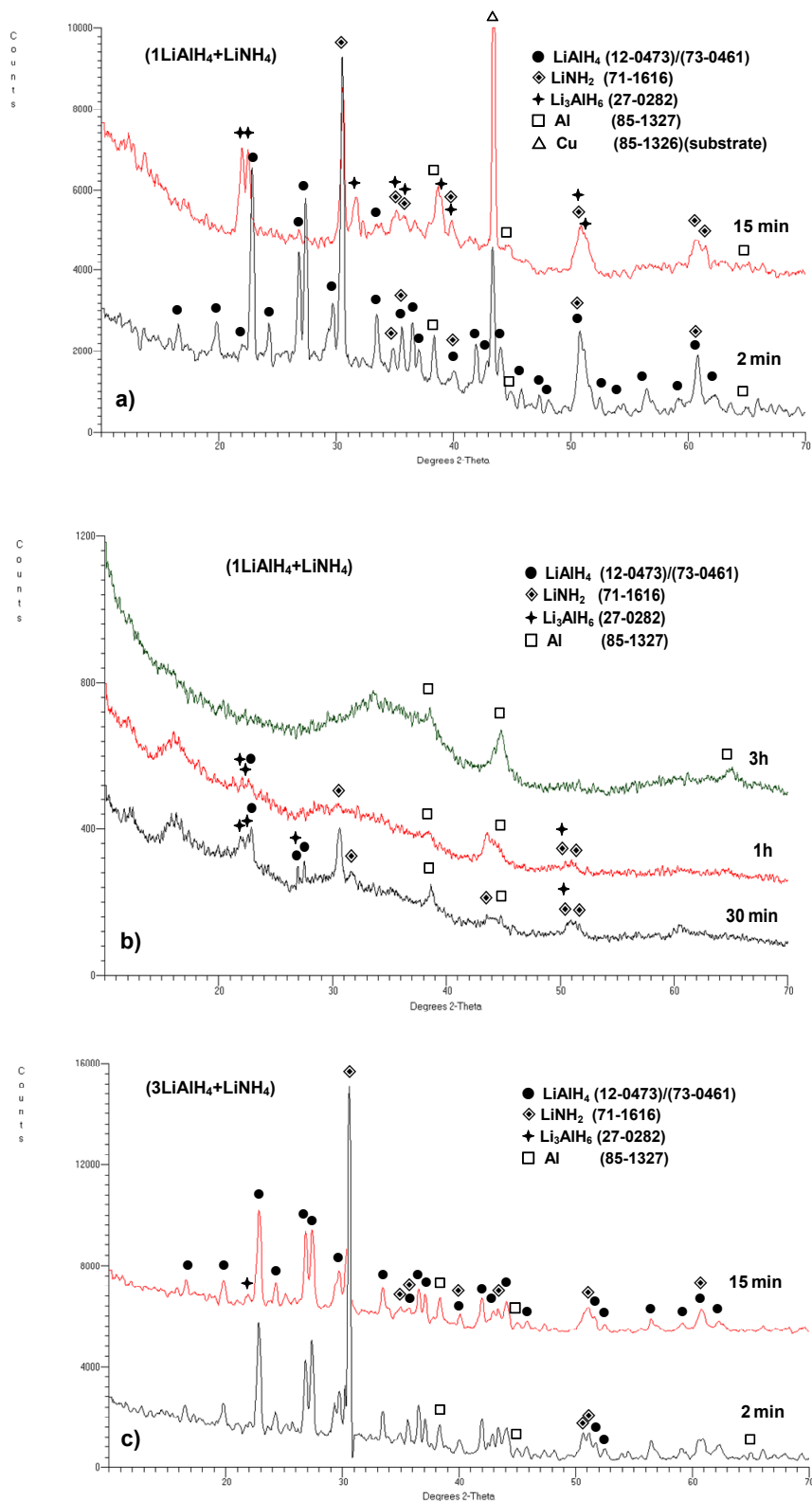
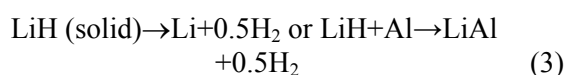
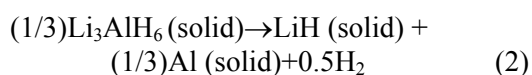
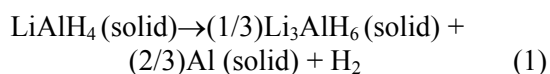


Figure 2. XRD patterns for (a) (1LiAlH<sub>4</sub>+LiNH<sub>2</sub>) after 2 and 15 min ball milling, (b) (1LiAlH<sub>4</sub>+LiNH<sub>2</sub>) after milling for 30min, 1h and 3h, and (c) (3LiAlH<sub>4</sub>+LiNH<sub>2</sub>) after milling for 2 and 15 min. The JCPDS file numbers for phase identification are shown in the legend

The XRD patterns in Figure 2 a, b show that from 2 min to 1h of milling duration the order of intensities for the peaks assigned to Al corresponds rather unambiguously to Al. However, the order of peak intensities changes after 3h of milling since the first peak assigned to Al in this pattern (Figure 2b) is weaker than the second one and also the third peak at around  $2\theta=65^\circ$  appears. This intensity order may correspond to AlN. However, the observed alterations in the intensities of peaks assigned to Al after 3h milling could also, at least to some extent, be induced by a severe nanostructuring or amorphization of the ball milled composite powders. Still, the maximum quantity of 5 wt. %  $H_2$  reproducibly observed after 3h of milling (Figure 1b) do not support the reaction path involving the formation of AlN, requiring 6.6 wt. %  $H_2$ , as claimed by Dolotko et al. [13]. The XRD patterns for the  $(3LiAlH_4+LiNH_2)$  ( $n=3$ ) composite after ball milling for 2 and 15 min (Figure 2c) still indicate the presence of both  $LiAlH_4$ ,  $LiNH_2$  and Al, the latter being still a pre-existing impurity. After 15 min milling a very small principal peak of  $Li_3AlH_6$  appears.

In general, it is well-known in the literature [1, 8-10] that the dehydrogenation of  $LiAlH_4$  in solid state occurs in three stages as shown below:



Only reactions (1) and (2) are accessible for practical hydrogen storage because they occur up to roughly  $250^\circ C$  in DSC tests. Reaction (3) occurs above  $400^\circ C$  and is of no interest [1, 8-10]. Theoretical  $H_2$  capacity of reaction (1) and (2) is 5.3 and 2.6 wt. %, respectively, which for 97% pure  $LiAlH_4$  in this work reduces to 5.14 and 2.52 wt. %, respectively. The composite with the molar ratio of  $n=1$  ( $1LiAlH_4+1LiNH_2$ ) corresponds to a weight ratio of 62.3 wt. %  $LiAlH_4$  and 37.7 wt. %  $LiNH_2$ . Therefore, at this weight ratio fully completed reaction (1) and (2) should provide approximately purity-corrected 3.2 and 1.6 wt. %  $H_2$ , respectively. Since  $\sim 5$  wt. %  $H_2$  is released after 150 min ball milling (Figure 1b) that means that both reactions

must have occurred during ball milling. This is a very interesting observation because reaction (1) is exothermic and (2) is endothermic [9, 10]. Apparently, both types of reactions can be realized during high energy ball milling of hydride composites in the present work.

Furthermore, it seems that the entire quantity of  $H_2$  desorbed during ball milling of the  $n=1$  composite (Figure 1b) could be easily provided by reaction (1) and (2) without invoking other reactions as claimed by Dolotko et al. [13]. The fact that the diffraction peaks of  $LiNH_2$  in the  $n=1$  composite persist throughout a long period of milling (Figure 2a, b) indicates that  $LiNH_2$  does not decompose but most likely is heavily nanostructured or even partially amorphous and in this capacity acts as a sort of catalyst which destabilizes  $LiAlH_4$  during ball milling and enhances its decomposition according to reaction (1) without involvement of any other reactions. However, with increasing molar content of  $LiAlH_4$  in the mixture ( $n=3$  and larger)  $LiNH_2$  somehow ceases to destabilize  $LiAlH_4$  during ball milling. At the content of 5 wt. % ( $n=11.5$ ) no release of  $H_2$  is observed (Figure 1b).

So far, such observations have never been reported in the literature. However, at the moment it is difficult to propose any detailed atomistic mechanism by means of which  $LiNH_2$  destabilizes  $LiAlH_4$  and, furthermore, the dependence of that mechanism on the molar ratio of the composite. Xiong et al. [11] pointed out that  $LiNH_2$  may not work as a simple catalyst. They tried to get more insight into the role of  $LiNH_2$  in the  $(0.5LiAlH_4+LiNH_2)$  composite using Nuclear Magnetic Resonance (NMR) and Infrared Fourier Transform (FTIR) measurements. They came to the conclusion that an intermediate with the approximate chemical composition of " $Li_3AlN_2H_4$ " was formed during milling. However, in their interpretation " $Li_3AlN_2H_4$ " is not really a new hydride but a mixture of  $(LiNH_2+AlN+2LiH)$  either amorphous or poorly crystalline. However, our XRD patterns in Figure 2a,b clearly show that the peaks of  $LiAlH_4$ ,  $Li_3AlH_6$ ,  $LiNH_2$  and Al are clearly observed up to 1h of high energy ball milling although they become progressively broader and weaker. Their persistent presence does not support the existence of any new intermediates. Also, their broadening/weakening is quite typical for progressive occurrence of nanostructuring and/or amorphization during ball milling.

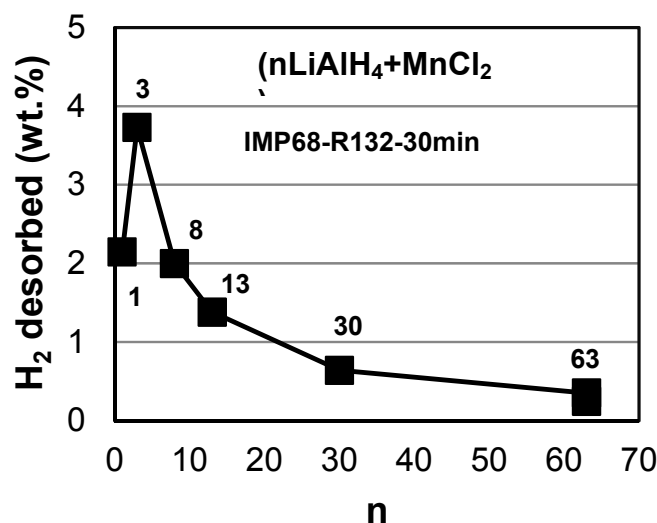


Figure 3. The quantity of H<sub>2</sub> desorbed during ball milling of (nLiAlH<sub>4</sub>+MnCl<sub>2</sub>) as a function of the molar ratio n (the numbers show the corresponding values of n)

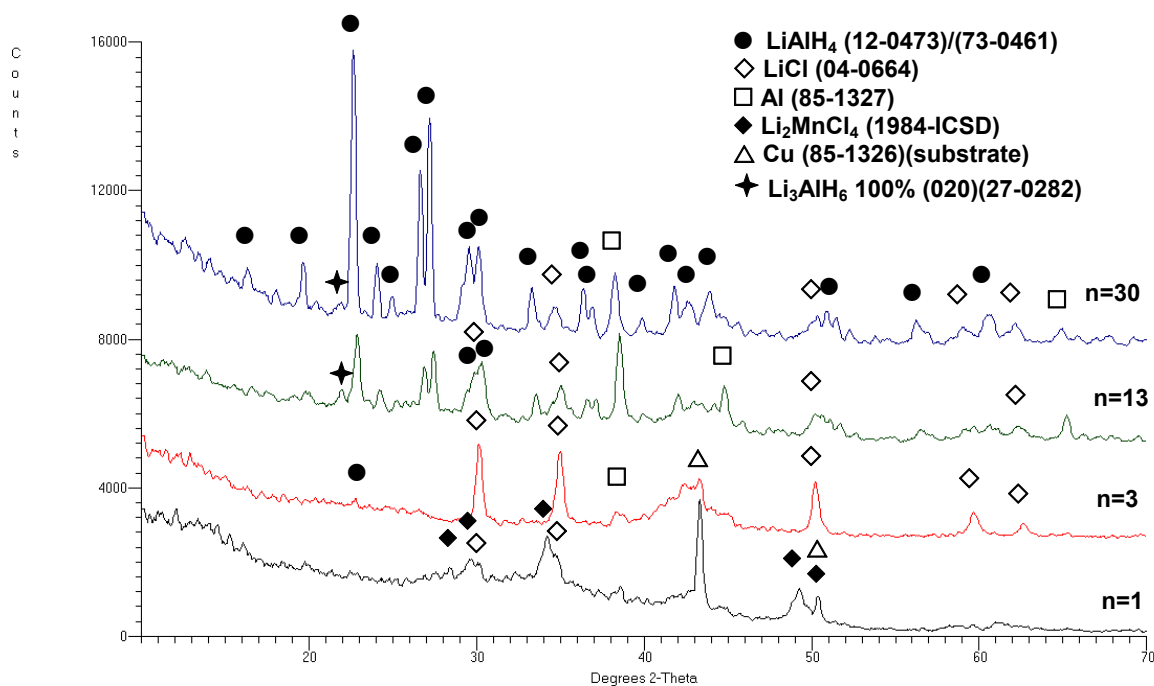


Figure 4. XRD pattern for the composite (nLiAlH<sub>4</sub>+MnCl<sub>2</sub>) with various molar ratios n, ball milled under IMP68-R132 for 30 min. The numbers of identification JCPDS files are given in the legend

### 3.2. Composite (nLiAlH<sub>4</sub>+MnCl<sub>2</sub>)

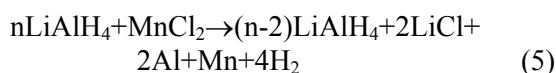
Figure 3 shows the quantity of H<sub>2</sub> desorbed during ball milling, plotted as a function of the molar ratio n of LiAlH<sub>4</sub> in the composite with MnCl<sub>2</sub>. This plot shows a similar general trend as Figure 1a, indicating that the maximum quantity of H<sub>2</sub>

released, occurs for n=3 and for higher n values, the H<sub>2</sub> quantity decreases with increasing n. The exception is n=1 for which the H<sub>2</sub> quantity desorbed during ball milling is smaller than that for n>1. That suggests that the composite with n=1 experiences a different H<sub>2</sub> release reaction than those with n>1. XRD phase analysis of the ball milled

( $n\text{LiAlH}_4 + \text{MnCl}_2$ ) for various  $n$  is shown in Figure 4. The XRD pattern for  $n=1$  reveals the presence of  $\text{Li}_2\text{MnCl}_4$  accompanied by a small amount of the secondary phase Al and possibly LiCl. This phase composition strongly suggests that the following principal reaction occurred during ball milling:



$\text{Li}_2\text{MnCl}_4$  is an inverse cubic spinel which has been extensively studied for its ionic conductivity as a potential solid electrolyte for lithium-ion batteries [14-16]. For the first time, our results show that this important compound can be relatively easily synthesized by ball milling. For  $n=1$  reaction (4) generates a theoretical amount of  $\sim 2.5$  wt. %  $\text{H}_2$  which agrees very well with 2.1 wt. %  $\text{H}_2$  released during ball milling for 97% pure  $\text{LiAlH}_4$  in Figure 3. Figure 4 shows that for  $n>1$  the LiCl peaks appear on the pattern which suggests the following reaction:



For  $n=2$  and 3 the above reaction should theoretically release 4.0 and 3.4 wt. %  $\text{H}_2$ , respectively. We did not investigate ball milling of the  $n=2$  composite but for  $n=3$  the quantity of  $\text{H}_2$  released during ball milling amounts to  $\sim 3.7$  wt.% (Figure 3), which agrees well with the theoretical capacity of reaction (5) for  $n=3$ . However, most likely  $\sim 0.3$  wt. %  $\text{H}_2$  in excess of reaction (5) is due to additional  $\text{H}_2$  release partially from reaction (1). In addition, for  $n=13$  and 30 a small (020) 100% intensity peak of  $\text{Li}_3\text{AlH}_6$  is also seen. This indicates that for large  $n$  reaction, (1) also occurs in which a small part of  $\text{LiAlH}_4$  is decomposing. Apparently reaction (1) and (5) can occur simultaneously although for small  $n$  reaction, (5) is the principal one. Since no diffraction peaks of Mn are observed on the XRD pattern after ball milling, most likely Mn is in an amorphous or highly nanocrystalline state. Also, it is seen in Figure 2 that the intensity of the  $\text{LiAlH}_4$  diffraction peaks increases with increasing  $n$  which means that the content of the  $\text{LiAlH}_4$  phase increases in the composite which agrees very well with reaction (5).

### 3.3. Composite ( $\text{LiNH}_2 + n\text{MgH}_2$ )

It is clearly seen in Figure 5a and b that the quantity of hydrogen desorbed during milling of ( $\text{LiNH}_2 + n\text{MgH}_2$ ) where  $n=1.0$  and 1.5 strongly depends on the milling energy and  $\text{MgH}_2$  molar ratio. Under a low energy shearing (LES6) mode, the composite with the ratio  $n=1$  does not desorb  $\text{H}_2$  under milling with 2&3 balls (Figure 5a) while it desorbs about 2 wt. %  $\text{H}_2$  after 25h of milling under

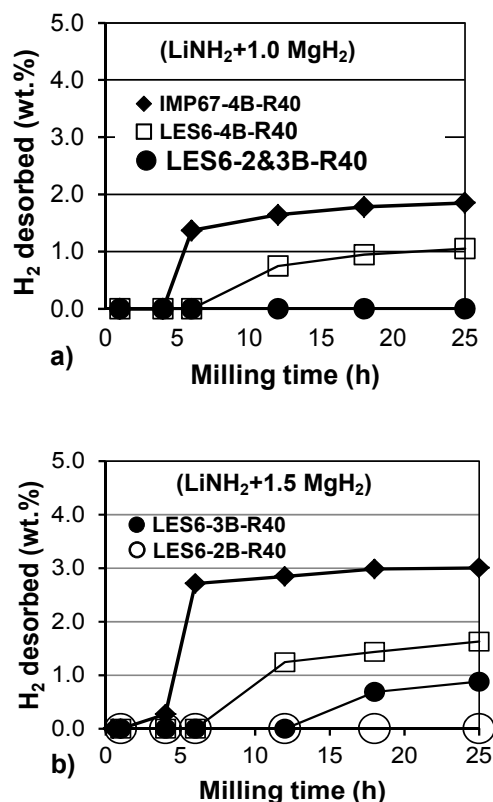


Figure 5. The quantity of  $\text{H}_2$  desorbed during ball milling under high energy impact (IMP67) and low energy shearing (LES6) modes as a function of milling time for (a) ( $\text{LiNH}_2 + 1.0\text{MgH}_2$ ) and (b) ( $\text{LiNH}_2 + 1.5\text{MgH}_2$ ) composite. B - the number of steel balls in the milling vial

high energy IMP67 mode. The composite with  $n=1.5$  starts desorbing  $\text{H}_2$  during milling under LES6-3B (3 balls) mode and releases  $\sim 3$  wt.%  $\text{H}_2$  after 25h of high energy milling under IMP67 mode. The XRD pattern in Figure 6a for  $n=1$  shows that low energy ball milling leads to the formation of LiH which coexists with retained  $\text{LiNH}_2$  and  $\text{MgH}_2$ .

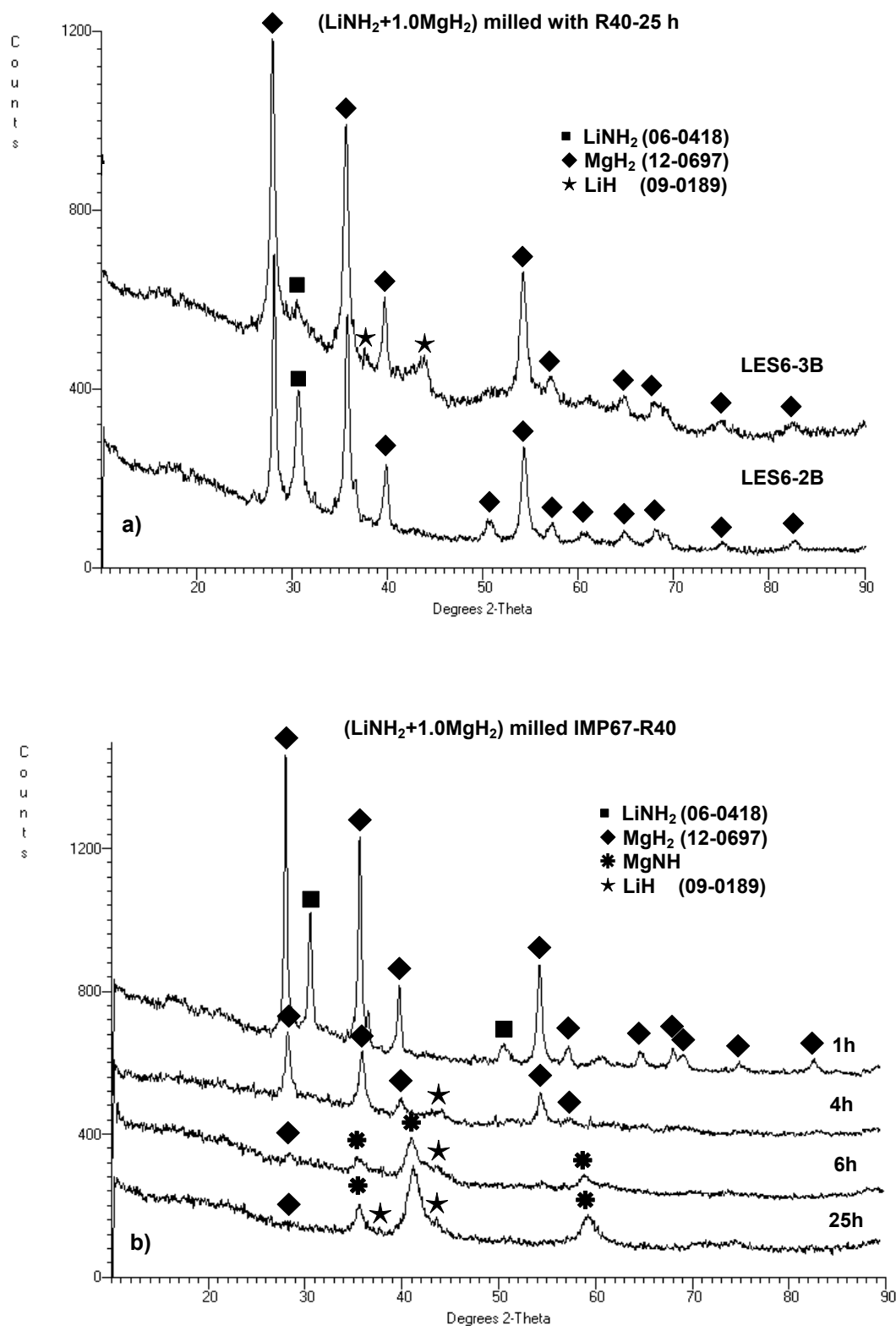


Figure 6. XRD patterns for the (LiNH<sub>2</sub>+1.0MgH<sub>2</sub>) (n=1) composite milled (a) for 25h under low energy mode (LES6) with 2 and 3 balls (2 and 3B) and (b) under high energy mode (IMP67 with 4 balls) for various times. The identification of MgNH hydride was done according to Ref. [17]

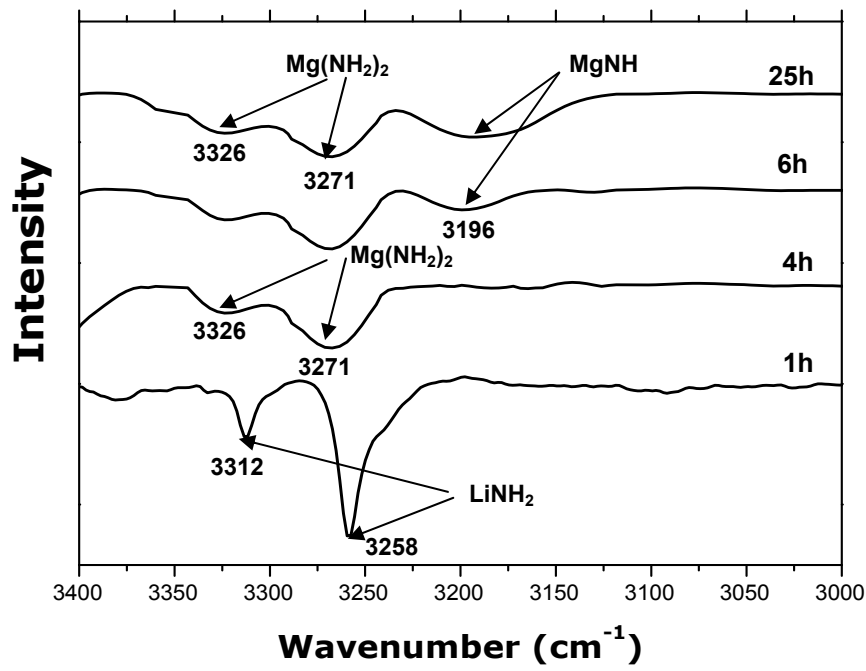


Figure 7. FT-IR absorption spectra for the  $(\text{LiNH}_2+1.0\text{MgH}_2)$  ( $n=1$ ) composite milled for various times (IMP67 mode) (identification of spectra according to [17])

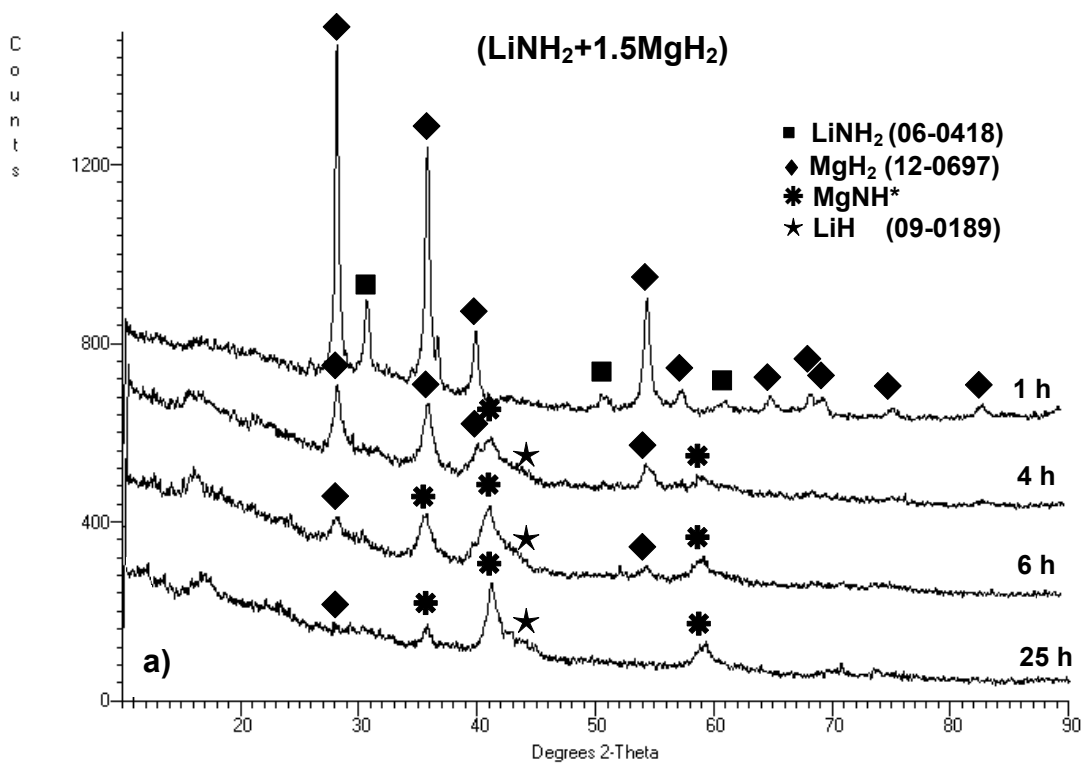


Figure 8a. XRD patterns for the  $(\text{LiNH}_2+1.5\text{MgH}_2)$  ( $n=1.5$ ) milled for various milling times (IMP67 mode) (identification of spectra and the  $\text{MgNH}$  phase according to [17]).

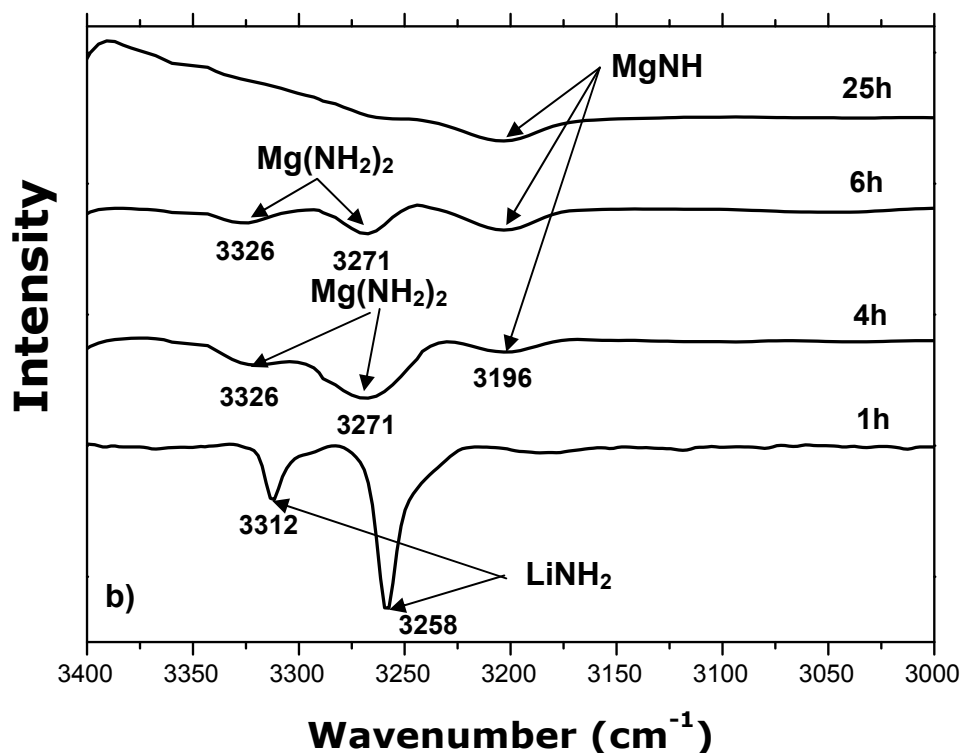
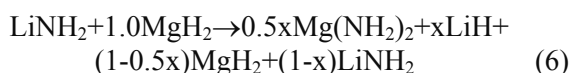


Figure 8b. FT-IR absorption spectra for the  $(\text{LiNH}_2+1.5\text{MgH}_2)$  ( $n=1.5$ ) milled for various milling times (IMP67 mode) (identification of spectra and the MgNH phase according to [17])

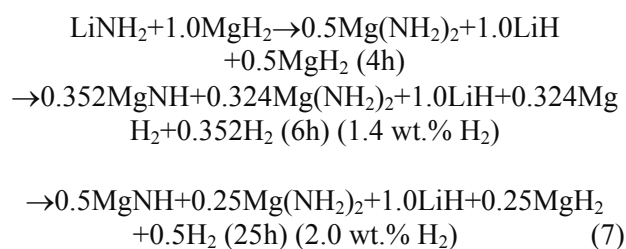
In addition, the Fourier-Transform Infrared Spectroscopy (FT-IR) showed that amorphous  $\text{Mg}(\text{NH}_2)_2$  (magnesium amide) was also present after low energy ball milling (the FT-IR spectra were similar to those in Figure 7 for IMP67 mode). Therefore, the following reaction which does not release  $\text{H}_2$  is proposed for the  $n=1$  composite milled under LES6-2B&3B low energy modes:



where  $x$  indicates that only fractions of  $\text{LiNH}_2$  and  $\text{MgH}_2$  are involved in the reaction since their diffraction peaks are still observed after ball milling (Figure 6a) and  $\text{Mg}(\text{NH}_2)_2$  is magnesium amide [17].

During high energy ball milling under IMP67 for 1h according to Figure 6b there is no reaction while milling for 4h results in the formation of LiH which indirectly indicates that also the formation of  $\text{Mg}(\text{NH}_2)_2$  occurred according to reaction (6). After even longer milling duration of 6 and 25h under high energy a new hydride identified as MgNH (magnesium imide) [17] is observed in the pattern. The Fourier-Transform Infrared Spectroscopy

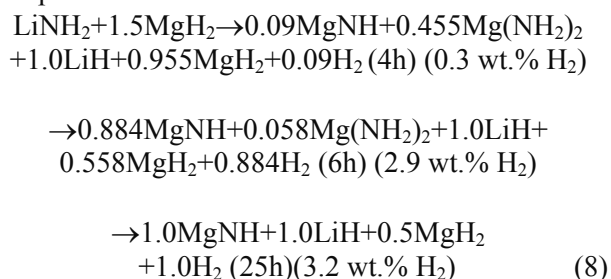
(FT-IR) spectra in Figure 7 show that amorphous  $\text{Mg}(\text{NH}_2)_2$  appears after 4h and the MgNH phase appears after 6h which confirms XRD analysis in Figure 6b. Therefore, the following sequence of reactions with increasing milling time without  $\text{H}_2$  release and accompanied by  $\text{H}_2$  release is proposed for the  $n=1$  composite:



The  $\text{H}_2$  capacities shown for each reaction are the theoretical ones and should be corrected for the purity of constituent hydrides to obtain the practical capacities observed in Figure 5a, although in practical terms both are very close to one another. For the  $n=1.5$  composite, the XRD patterns for milling time 1, 4 6 and 25h under high milling energy mode (IMP67) are shown in Figure 8a. The LiH and MgNH phases appear after 4h of ball milling. The presence of LiH is associated with the

formation of  $\text{Mg}(\text{NH}_2)_2$  according to reaction (6). The Fourier-Transform Infrared Spectroscopy (FT-IR) in Figure 8b shows that both the amorphous  $\text{Mg}(\text{NH}_2)_2$  (magnesium amide) and crystalline  $\text{MgNH}$  phases are present after 4h of ball milling which confirms XRD phase analysis.

Therefore, the following sequence of reactions with increasing milling time without  $\text{H}_2$  release and accompanied by  $\text{H}_2$  release is proposed for the  $n=1.5$  composite:



The  $\text{H}_2$  capacities shown are the theoretical ones and should be corrected for the purity of constituent hydrides to get the practical ones observed in Figure 5b.

#### 4. DISCUSSION

Finally, it must be pointed out that the transformation pathways induced by mechano-chemical reactions accompanied by  $\text{H}_2$  release or no  $\text{H}_2$  release during ball milling are solely enabled by the true compositing associated with the profound changes in the microstructure of powders, occurring side by side during ball milling, which lead to the formation of nanomaterials. It must be stressed that these reactions have not been observed in simple mixtures with the same molar ratios in which the hydride constituents were simply mixed by mortar and pestle. For example, the measured Specific Surface Area (SSA) of the ball milled ( $\text{LiNH}_2 + 1.0\text{MgH}_2$ ) composite increases with increasing ball milling energy from 2.4 to 29.8, 37.3 and 52.0  $\text{m}^2/\text{g}$  after 25h of ball milling under LES6-2B, LES6-3B and IMP68 (4 balls) mode, respectively. Low Energy Shearing (LES) mode is a low-energy milling mode. The SSA increase is obviously related to the profound reduction of powder particle size. Simultaneously, the grain size within the  $\text{LiNH}_2$  powder particles in the composite is reduced to about 60 nm (after 1h milling) and 20 nm (after 25h) [18]. The  $\text{MgH}_2$  grain (crystallite) size is reduced to 30 nm (after 15 min milling) and 10 nm (after 1h) [1, 7]. This formation of

nanocrystalline hydride sequence during ball milling is characteristic for every hydride system studied.

#### 5. CONCLUSIONS

Large quantities of hydrogen ( $\text{H}_2$ ) are observed to be released/desorbed at ambient temperatures during the mechano-chemical synthesis of the Li-Al-N-Mg-based hydride composites using an energetic ball milling in a unique magneto-mill. In the ( $n\text{LiAlH}_4 + \text{LiNH}_2$ ;  $n=1, 3, 11.5$  and 30) composite the largest quantity of about 5 wt. %  $\text{H}_2$  is released for the molar ratio  $n=1$ . The released  $\text{H}_2$  quantity decreases with increasing  $n$  value. XRD tests do not provide any tangible evidence for reactions between the constituent hydrides in the composite. It seems that at the molar ratio  $n=1$ , the  $\text{LiNH}_2$  constituent acts as a sort of catalyst destabilizing  $\text{LiAlH}_4$  during ball milling and enhancing its decomposition to  $\text{Li}_3\text{AlH}_6$  and Al and then  $\text{Li}_3\text{AlH}_6$  to LiH and Al. Both decomposition pathways are associated with  $\text{H}_2$  release. With increasing molar content of  $\text{LiAlH}_4$  in the mixture up to  $n=3$  and greater,  $\text{LiNH}_2$  somehow ceases to destabilize  $\text{LiAlH}_4$  during ball milling anymore.

In the ( $n\text{LiAlH}_4 + \text{MnCl}_2$ ;  $n=1, 3, 8, 13, 30$  and 63) composite the maximum quantity of  $\text{H}_2$  released occurs for  $n=3$  and then the  $\text{H}_2$  quantity decreases with increasing  $n$ . For  $n=1$ , the quantity of  $\text{H}_2$  desorbed during ball milling is smaller than that for  $n=3$ . XRD phase analysis shows that for the composite with  $n=1$  dehydrogenation reaction during ball milling which occurs between the hydride and chloride constituent, forms an inverse cubic spinel  $\text{Li}_2\text{MnCl}_4$ . In contrast, for  $n>1$ , the formation of lithium salt ( $\text{LiCl}$ ) and also a partial decomposition of  $\text{LiAlH}_4$  can occur simultaneously. In the ( $\text{LiNH}_2 + n\text{MgH}_2$ ;  $n=1.0$  and 1.5) composite, the pathway of hydride reactions depends on the milling energy and milling time. Under low milling energy up to 25h, there is either no reaction (1h) or the reaction products are amorphous  $\text{Mg}(\text{NH}_2)_2$  (magnesium amide) and nanocrystalline LiH (lithium hydride) without release of hydrogen. Under high milling energy, a new hydride  $\text{MgNH}$  (magnesium imide) is formed due to the reaction between  $\text{Mg}(\text{NH}_2)_2$  and  $\text{MgH}_2$  which is always associated with the release of  $\text{H}_2$ .

## ACKNOWLEDGEMENTS

This research was supported by the NSERC Hydrogen Canada (H2CAN) Strategic Research Network and NSERC Discovery grants which are gratefully acknowledged. The authors are grateful to Prof. Linda Nazar from the Department of Chemistry, University of Waterloo, for the usage of XRD equipment. The authors thank Dr. Z.S. Wronski from the CanmetENERGY, Natural Resources Canada for the BET particle size measurements of the (LiNH<sub>2</sub>+1.0MgH<sub>2</sub>) composite.

## REFERENCES

- [1] Varin, R.A., Czujko, T., Wronski, Z. S., *Nanomaterials for Solid State Hydrogen Storage*, Springer Science+Business Media, New York, 2009
- [2] Dillich, S., *D.O.E. Hydrogen Program 2009 Annual Progress Report*, IV.0 Hydrogen Storage Sub-Program Overview, May 2009
- [3] Varin, R. A., Zbroniec, L., *The Effects of Nanometric Nickel (Ni) Catalyst on the Dehydrogenation and Rehydrogenation Behavior of Ball Milled Lithium Alanate (LiAlH<sub>4</sub>)*, Journal of Alloys and Compounds, Vol. 506 (2010), p. 928-939
- [4] Varin, R. A., Zbroniec, L., Czujko, T., Wronski, Z. S., *The Effects of Nanonickel Additive on the Decomposition of Complex Metal Hydride LiAlH<sub>4</sub> (lithium alanate)*, International Journal of Hydrogen Energy, Vol. 36 (2011), p. 1167-1176
- [5] Varin, R.A., Zbroniec, L., *Decomposition Behavior of Unmilled and Ball Milled Lithium Alanate (LiAlH<sub>4</sub>) Including Long-Term Storage and Moisture Effects*, Journal of Alloys and Compounds, Vol. 504 (2010), p. 89-101
- [6] Varin, R. A., Zbroniec, L.: *The Effects of Ball Milling and Nanometric Nickel Additive on the Hydrogen Desorption from Lithium Borohydride and Manganese Chloride (3LiBH<sub>4</sub>+MnCl<sub>2</sub>)*, International Journal of Hydrogen Energy, Vol. 35 (2010), p. 3588-3597
- [7] Varin, R. A., Czujko, T., Wronski, Z. S.: *Thermal Stability of Vale Inco Nanometric Nickel as a Catalytic Additive for Magnesium Hydride (MgH<sub>2</sub>)*, International Journal of Hydrogen Energy, Vol. 34 (2009), p. 8603-8610
- [8] Varin, R. A., Zbroniec, L.: *Decomposition Behavior of Unmilled and Ball Milled Lithium Alanate (LiAlH<sub>4</sub>) Including Long-term Storage and Moisture Effects*, Journal of Alloys and Compounds, Vol. 504 (2010), p. 89-101
- [9] Varin, R. A., Zbroniec, L.: *The Effects of Nanometric Nickel (Ni) Catalyst on the Dehydrogenation and Rehydrogenation Behavior of Ball Milled Lithium Alanate (LiAlH<sub>4</sub>)*, Journal of Alloys and Compounds, Vol. 506 (2010), p. 928-939
- [10] Varin, R.A., Zbroniec, L., Czujko, T., Wronski, Z. S., *The Effects of Nanonickel Additive on the Decomposition of Complex Metal Hydride LiAlH<sub>4</sub> (Lithium Alanate)*, International Journal of Hydrogen Energy, Vol. 36 (2011), p. 1167-1176
- [11] Xiong, Z., Wu, G., Hu, J., Chen, P., *Investigation on Chemical Reaction Between LiAlH<sub>4</sub> and LiNH<sub>2</sub>*, Journal of Power Sources, Vol. 159 (2006), p. 167-170
- [12] Xiong Z., Wu G., Hu, J., Liu, Y., Chen, P., Luo, W., Wang, J., *Reversible Hydrogen Storage by a Li-Al-N-H Complex*, Advanced Functional Materials, Vol. 17 (2007), p. 1137-1142
- [13] Dolotko, O., Zhang, H., Ugurlu, O., Wiench, J. W., Pruski, M., Chumbley, L. S., Pecharsky, V., *Mechanochemical Transformations in Li(Na)AlH<sub>4</sub>-Li(Na)NH<sub>2</sub> Systems*, Acta Materialia, Vol. 55 (2007), p. 3121-3130
- [14] Van Loon, C. J. J., de Jong, J., *Some Chlorides with the Inverse Spinel Structure: Li<sub>2</sub>TCl<sub>4</sub> (T=Mg, Mn, Fe, Cd)*, Acta Crystallographica, Vol. B31 (1975), p. 2549-2550
- [15] Court-Castagnet, R., Kaps, Ch., Cros, C., Hagenmuller, P., *Ionic Conductivity-Enhancement of LiCl by Homogeneous and Heterogeneous Dopings*, Solid State Ionics, Vol. 61 (1993), p. 327-334
- [16] Robertson, A. D., West, A., R., Ritchie, A., G., *Review of Crystalline Lithium-Ion Conductors Suitable for High Temperature Battery Applications*, Solid State Ionics, Vol. 104 (1997), p.1-11
- [17] Liang, C., Liu, Y., Luo, K., Li, B., Gao, M., Pan, H., Wang, Q., *Reaction Pathways Determined by Mechanical Milling Process for Dehydrogenation/Hydrogenation of the LiNH<sub>2</sub>/MgH<sub>2</sub> System*, Chemistry - A European Journal, Vol. 16 (2010), p. 693-702
- [18] Varin, R. A., Jang, M., Polanski, M., *The effects of ball milling and molar ratio of LiH on the hydrogen storage properties of nanocrystalline lithium amide and lithium hydride (LiNH<sub>2</sub>+LiH) system*, Journal of Alloys and Compounds, Vol. 491 (2010), p. 658-667

Received: 11. 11. 2011.

Accepted: 11. 11. 2011.

Authors' address

Robert A. Varin

Minchul Jang

Department of Mechanical and Mechatronics Engineering, University of Waterloo

200 University Ave. W.

Waterloo

Ontario

Canada N2L 3G1

Leszek Zbronic

Wroclaw Research Centre EIT+

Stablowicka 147

54-066 Wroclaw

Poland

ravarin@uwaterloo.ca

leszek.zbronic@hotmail.com

m2jang@engmail.uwaterloo.ca

